

Corrosion of Cu-Base Alloys in Geothermal Condensates

M. Ko and K. A. Lichti

Quest Reliability Ltd., Gracefield Research Centre, Lower Hutt, New Zealand

m.ko@questreliability.com and k.lichti@questreliability.com

Keywords: copper, brass, H_2S , corrosion, geothermal, condensate, aeration, iron inhibition

ABSTRACT

Copper base alloys have excellent heat transfer properties but have had limited application in geothermal waters because of the risk of H_2S corrosion and the risk of copper contamination of ferrous materials.

The results of copper and Al-brass coupon exposure trials in H_2S containing geothermal steam condensates completed at the Broadlands-Ohaaki geothermal well BR22 are reported. Corrosion coupons exposed in steam condensate show presence of iron and stable corrosion products indicating impact of corrosion of the carbon steel test chamber - iron injection is known to lower corrosion of copper alloys in cooling waters. Deliberate contamination of one of the test chambers with air resulted in a higher corrosion rate. Thermodynamic models of the damage mechanisms are presented.

1. INTRODUCTION

Carbon steel and stainless steels are generally used in geothermal environment mostly due to their individual corrosion resistant properties; but for aggressive geothermal environments the more corrosion resistant materials required are generally much more expensive. Copper and its alloys have excellent heat transfer properties and would be economically viable materials for use for specialised applications in geothermal environment if their corrosion resistance was adequate.

Copper alloys have been previously used as brazing materials for heat exchanger, heat exchanger tubes, heat pumps, boilers and as a part of specialised control valves (Miller (1979), Akol'zin et al (1973), and Raferty (1989)). Raferty (1993) reported the performance of copper tubing in some geothermal fluids such as at Boise, ID where lifetime as long as ten years was observed; but other sites such as at Pagosa Spring, CO had aggressive reactions that lead to failures as early as two years in service. Wall thinning and perforation of copper tubing has been attributed to corrosion attack of hydrogen sulfide (H_2S). Since most geothermal fluids contain hydrogen sulfide

(H_2S) or ammonia (NH_3), copper and its alloys are generally avoided.

Corrosion coupon exposure experiments were performed in Broadlands geothermal well BR22, New Zealand. This report summarises the results of the performance of copper and its alloys in the condensate environments. A common concern with the use of copper is the dissolution and transport of copper ions onto ferrous materials resulting in galvanic couples. This work did not attempt to replicate this effect.

2. TEST ENVIRONMENT CHEMISTRY

Corrosion investigations were initiated in 1976 the Chemistry Division of Department of the Scientific and Industrial Research (DSIR). This investigation tested 36 different ferrous and non ferrous alloys for use in a geothermal power plant in Broadlands, New Zealand. Three different exposure periods were tested, 4 weeks, 13 weeks and 52 weeks. Braithwaite and Lichti (1980) reported the initial results of the investigation.

The test coupons had a minimum exposed surface area of $0.23dm^2$ and were prepared according to the ASTM Recommended Practice for Preparing, Cleaning and Evaluating Corrosion Test Specimens (G 1-72) and the ASTM Recommended Practice for Conducting Plant Corrosion Tests (G 4-68 (1974)). A corrosion rig was constructed on the site of Broadlands geothermal well BR22 to study the corrosion of semi-static environment exposures of metal coupons in seven different environments. A summary of the environmental conditions is shown in Table 1 and the summary of the test environment chemical conditions is shown in table 2.

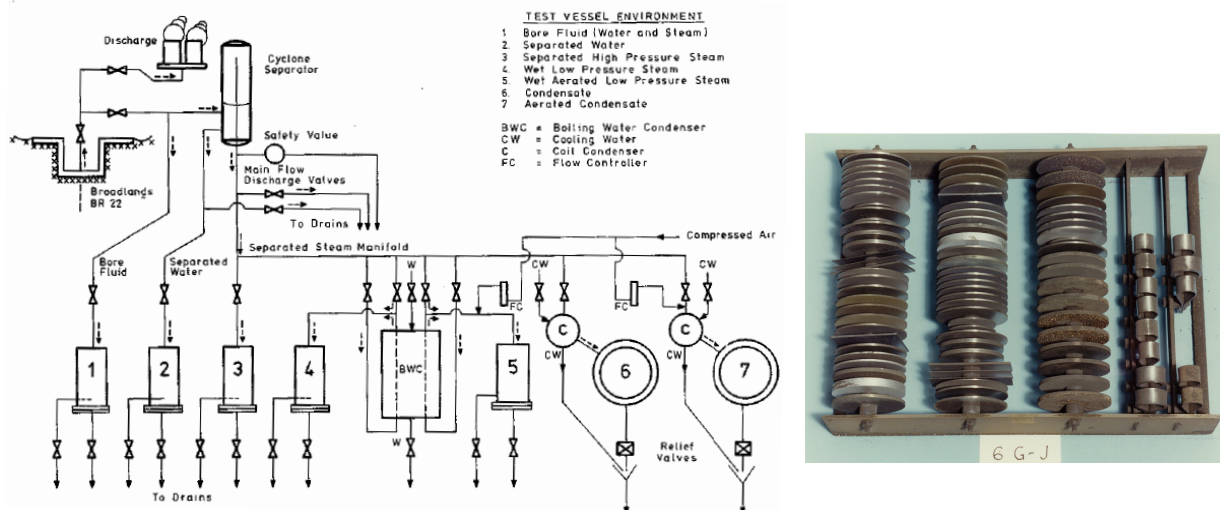
Geothermal bore fluid was extracted from Well BR22 and a cyclone separator was used to separate the bore water from high-pressure steam (**Error! Reference source not found.** Figure 1a). The steam was used as supply for the rest of the plant for other corrosion testing. For Vessels 6 and 7 (cold condensate and aerated cold condensate respectively), the steam was condensed using water cooled coil condensers. In Vessel 7, three percent by volume of air was added to the steam before condensation to simulate an aerated condensate environment.

Table 1: Summary of various test environment conditions, adapted from Braithwaite and Lichti (1980).

Vessel	Description	Environment			
		Pressure (kPa)	Temp (degC)	Mass Flow (kg/h)	Fluid Vel (dm/min)
1	Bore Fluid (water+steam)	650	160	178	14.5
2	Separated Bore Water	650	156	56	0.2
3	Separated HP Dry Steam	650	160	40	11.6
4	Wet LP Steam (10%wet)	126	105	57	215.6
5	Wet LP Aerated Steam (10%wet+3%air)	135	106	32	129.9
6	Cold Condensate	300	10-20	14	0.012
7	Aerated Cold Condensate (3%air)	135	10-20	12	0.01

Table 2: Summary of corrosion test environments chemical conditions, adapted from Braithwaite and Lichti (1980)

Vessel	Test Environment	pH	Condensed Fluid Conductivity S/m x 10 ⁻²	Chemical Species, mmol/litre				
				H ₂ S	SO ₄	NH ₃	CO ₂	Fe
2	Separated Bore Water	7.50	4.00	0.32	0.10	0.28	?	nil
3	Separated HP Steam ^a	5.70	2.20	9.50	nil	2.35	475	nil
4	Wet LP Steam			9.6 ^b				
5	Wet LP Aerated Steam			11.4 ^b				
6	Cold Condensate	5.15	1.92	2.4	0.004	2.35	48.2 ^c	0.226
7	Aerated Cold Condensate	6.00	2.33	0.23	0.14	2.24	8.1 ^c	0.204

^a Sampled before passing through the corrosion vessel.^b High H₂S in aerated stream due to the collection method, during which steam was lost^c Calculated

a. Schematic diagram of corrosion rig constructed in Broadlands, NZ.



b. Pictures of coupons on a loaded rack for exposure inside Vessel 6, Cold Condensate.

Figure 1: Schematic diagram of corrosion rig in Broadlands, New Zealand. Vessel 6 coupons shown after 12 months.

The condensate pressure vessels were vertically oriented and constructed from mild steel with capacity of three racks (229 x 305 mm). Diffuser plates were used to prevent direct impingement of incoming fluids on exposed coupons. Racks were made up of prepared coupons, supported on rods sleeved with polytetrafluoroethylene (PTFE) and separated by insulating spacers of the same material (Figure 1b). It was then inserted into the specially designed holders in the vertical vessels. After exposure, the racks holding the coupons were washed at once in hot water and dried at 110°C. After cooling, the racks were stored in polyethylene bags containing a desiccant, until disassembled under controlled laboratory conditions.

This report describes results for two materials exposed as part of that work, namely an alloy designated as 41-103 a Deoxidised Copper (>99.5% Cu) and an alloy designated as B8 an Aluminium Brass (2.1% Al, 20.5% Zn, <0.1% Mn/Si/Fe/Ni). Only the cold condensate environments, Vessel 6 (deaerated) and Vessel 7 (aerated) are reported.

3. EXPERIMENTAL PROCEDURE

3.1 Corrosion Product Characterisation

The uncleaned coupon samples were visually inspected and detailed analysis of the corrosion product characterisation was performed using Scanning Electron Microscopy (SEM) and X-ray Diffraction (XRD). SEM-EDX analysis was used

to determine the structure (morphology) and composition of the surface corrosion products of the samples.

An ESEM: FEI Quanta 200F and a Philips FEG SEM instruments were used. Energy Dispersive X-ray analysis (EDX) of the SEM was used to identify elemental composition in the corrosion products. XRD characterisation (both in situ and removed and powdered sample) was used to determine the crystalline compounds present in the corrosion products.

3.2 Thermodynamic Analysis

Potential - pH (Pourbaix) diagrams were formulated using the aid of thermodynamic software HSC Chemistry 5.

4. RESULTS

Exposed duplicate coupons were analysed as follows:

- One of each was cleaned of all corrosion products using 10% H₂SO₄ and 50g/L KCN solution.
- One of each was subjected to metallurgical analysis.

4.1 Corrosion Rates

Corrosion rates were calculated using the material loss method on cleaned metal coupons after exposure. Material loss method was employed because of the layered structure of corrosion products that often flaked off. In other

instances, foreign material contaminated the corrosion products and these effects are eliminated from the mass loss by chemically removing the formed corrosion products.

The rate of corrosion was calculated using the weight loss method. Material loss was defined as the mean thickness of the material lost by corrosion during an exposure period:

$$ML = (\delta / \rho A) \times 10^3, \quad (1)$$

where ML = Material loss (μm); δ = Weight loss (mg), ρ = Material density (mg/mm^3) and A = Exposed area of test material (mm^2).

Corrosion rate was calculated as follow:

$$CR = (ML \times \text{constant}) / t, \quad (2)$$

where CR = Corrosion rate ($\mu\text{m/yr}$), ML = Material loss (μm), $\text{constant} = 31.557 \times 10^6$ (s/mean solar yr) and t = Exposure period (s).

The results obtained suggested an approximately linear to semi parabolic corrosion rate for both materials as illustrated in Figure 2. Linearly increasing material loss was observed for copper material in cold condensate (Vessel 6) and brass material in the aerated condition (Vessel 7). The linear rate loss suggests a minimum of protective film was formed. The material loss of copper in the aerated condition was at of an order of a magnitude higher than that found in the non-aerated condition.

In the non-aerated condensate environment, the addition of alloying elements significantly decreased the rate of corrosion by about an order of a magnitude. The same effect was not observed in the aerated condition. The material loss of brass in the aerated condition (Vessel 7) was at least two orders of magnitudes higher than those found in the non-aerated condition (Vessel 6).

Brass material in the cold condensate environment, showed two different corrosion mechanisms, initially showing a linear rate loss which then changed to a parabolic rate loss at longer exposure periods. It can be argued that some protective film was formed.

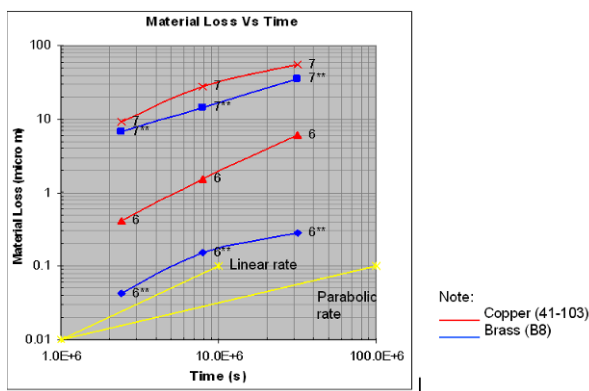


Figure 2: Graph of material loss of Copper and Al Brass in geothermal condensates for 4, 13 and 52 weeks. 6 and 7 = Copper. 6'' and 7'' = Brass.

4.2 Pitting Results

Corrosion pits were observed on all of the copper and brass coupons. Pit densities and pit depths on the samples were measured according to ASTM Recommended Practice for Examination and Evaluation of Pitting corrosion (G46-76). Summaries of the pitting results are given in Table 3.

Under non-aerated condition of Vessel 6, the pit density on the copper and aluminium brass coupons increased over time. However, the formation and propagation of these pits changed after prolonged exposure, so there was a high density of shallower pits observed. The pitting corrosion examined appeared to be very uniform. Most of the coupons show a step from corrosion near to the crevice areas.

The pit depth and pit density of copper and aluminium brass coupons exposed to aerated condition in Vessel 7, were much higher compared to coupons exposed to non-aerated condition. Corrosion attack was non-uniform and local areas of pitting were observed. Maximum pit depth on the copper coupons was measured to be 182 μm at 52 weeks exposure period. Localised accelerated attack was observed at the edge of the crevice area forming corrosion channels. Channels were deepened over time but changed to more general corrosion at prolong exposure.

Table 3: Pitting data of copper based alloys coupons exposed in geothermal condensates.

Copper (41-103)					
Vessel No	Time	Location	Pit Depth		Pit Density ASTM G46
			Avg (μm)	Max (μm)	
V 6	4 weeks	Face	66	88	large pits A2 *
		Crevice	13	18	A1
	13 weeks	Face	57	73	large pits A3
		Crevice	15	20	A2
	52 weeks	Face	25	31	A5
		Crevice	10	13	small pits A2
	4 weeks	Face	55	59	A5**
		Crevice	30	44	A2
V 7	13 weeks	Face	98	120	A5**
		Crevice	38	55	A3
	52 weeks	Face	130	182	A5**
		Crevice	52	100	A2
Al Brass (B8)					
Vessel No	Time	Location	Pit Depth		Pit Density ASTM G46
			Avg (μm)	Max (μm)	
V 6	4 weeks	Face	42	55	A2
		Crevice	14	15	A2
	13 weeks	Face	42	65	large pits A3
		Crevice	12	18	A2
	52 weeks	Face	25	65	A5
		Crevice	5	8	A5
	4 weeks	Face	46	114	A5
		Crevice	24	30	A3
V 7	13 weeks	Face	70	96	A5**
		Crevice	52	72	A3
	52 weeks	Face	84	98	A5**
		Crevice	70	93	A5

Note: Pits with greatest depth were selected for measurement

* small pits initiated A5

** non uniform

4.3 Corrosion Product Characterisation

Summaries of coupons analysed for this work is given in Table 4 for clarification.

Table 4: Coupons summary.

Time	Copper		Al Brass	
	V 6	V 7	V 6	V 7
4 weeks	-	CuB7B	-	B8B7B
13 weeks	CuB6E	CuB7D	B8B6E	B8B7E
52 weeks	CuB6H	CuB7H	B8B6H	B8B7H

Note: V6 – Vessel 6 (Cold Condensate)

V7 – Vessel 7 (Aerated Cold Condensate)

4.3.1 Deoxidised Copper 41-103 Coupons

Copper coupon samples from the cold condensate environment exposed for 13 weeks (sample CuB6E) and 52 weeks (sample CuB6H) were selected for metallurgical analysis. Corrosion products uniformly covered the entire surface area of both coupon samples. Brown corrosion products observed on sample CuB6E had a powder like

deposit that could be easily rubbed off. Sample CuB6H showed dark brown/black coloured adherent corrosion products with fine-grained appearance.

SEM examination revealed that after the 13 weeks exposure period, the corrosion products were mainly in the form of plate-like structure and fine spherical agglomerates (Figure 3). The fine spherical agglomerates appeared to have been precipitated out of solution, which then deposited on the top of the plate like corrosion product. The glassy plate like corrosion products showed predominance of copper (Cu) and sulphur (S) with a lower level of oxygen (O) and iron (Fe), suggesting copper-sulfide compounds. Analysis of the fine spherical agglomerate (Figure 3) showed a higher level of iron (Fe). Trace amount of arsenic (As) and antimony (Sb) typical of geothermal solutions were also detected in some areas. It should be noted that the presence of iron in the corrosion product was not originally expected. Iron was attributed to the corrosion of the test vessel itself.

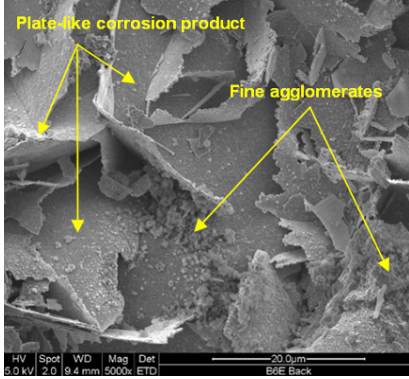


Figure 3: SEM image of CuB6E surface corrosion product.

The cross section of sample CuB6E showed a thin corrosion product layer next to the metal interface with thickness ranging in between 2 to 5 μm. Corrosion product crystal growth with similar elemental compositions can also be observed which corresponded with the surface topography. In some areas, flat corrosion products of around 10 μm in thickness were observed. These formed a layered structure with a higher iron level detected in between the layers.

XRD spectrum of Sample CuB6E revealed that the outer surface of the corrosion products was mainly crystalline. The crystalline phases detected were chalcosite (Cu_2S), bornite (Cu_5FeS_4) and chalcopyrite (CuFeS_2).

At 52 weeks, the sample generally had larger particles than those observed in the 13 weeks exposure (Figure 4). The corrosion products observed were in the form of plate like and acicular needle structures. The plate like material showed a similar composition to that found in the 4 week sample, with predominance of copper (Cu) and sulphur (S). Analysis of the acicular corrosion product revealed a high iron (Fe) content (similar to the fine spherical agglomerate structure found in the 13 week sample).

Cross sections of sample CuB6H showed three distinct layers of corrosion product (Figure 4). Over time, a significant increase in the thickness of the corrosion products was observed. The thickness of the first layer of corrosion product next to the copper metal interface was measured to be between 9 to 15 μm. The light grey areas appeared to be mainly copper sulphides (Cu_2S). The brown areas observed in the next layer were analysed to contain a

high level of copper (Cu) with almost equal amounts of sulphur (S) and iron (Fe) which predominantly suggested a copper iron sulphide (CuFeS_2).

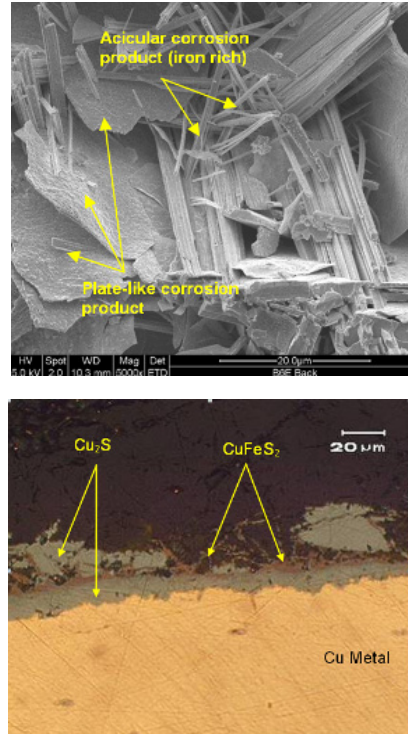


Figure 4: SEM images of the surface morphology and optical image of cross section of sample CuB6H.

These results were supported by the XRD analysis performed on the surface of the sample. XRD results showed that Sample CuB6H was predominantly crystalline with the major compounds present being chalcosite (Cu_2S) and copper iron sulphide ($\text{Cu}_{17.6}\text{Fe}_{17.6}\text{S}_{32}$).

Vessel 7 tested the effect of aeration on copper performance. Coupons exposed for 4 weeks (sample CuB7B), 13 weeks (sample B7D) and 52 weeks (sample CuB7H) were subjected to metallurgical analysis. Thin black corrosion products covered the entire surface area of sample CuB7B. The corrosion products observed were adherent to the copper parent metal with some areas of partial flaking exposing a second layer, this being yellow coloured corrosion product. With longer exposure period, the corrosion products appeared to be thicker and more readily flaked off with some areas of brown corrosion product thought to be due to air oxidation.

At 4 weeks exposure to the aerated condition, the corrosion appeared to be crystalline (Figure 5) with fine particles on the second layer (Figure 5). SEM analysis on the black top layer of the corrosion products showed high levels of copper (Cu) and sulphur (S) with a lower level of oxygen (O) detected. The green second layer of the corrosion product showed presence of mainly copper (Cu) and oxygen (O). Low levels of iron (Fe) were detected in some spots.

The cross section showed areas where corrosion products were detached or completely flaked off from the copper metal and newly formed thin corrosion product observed on the metal surface. Where corrosion products were adherent, cracks on the interface were commonly encountered evidencing the non-protective properties of the formed films.

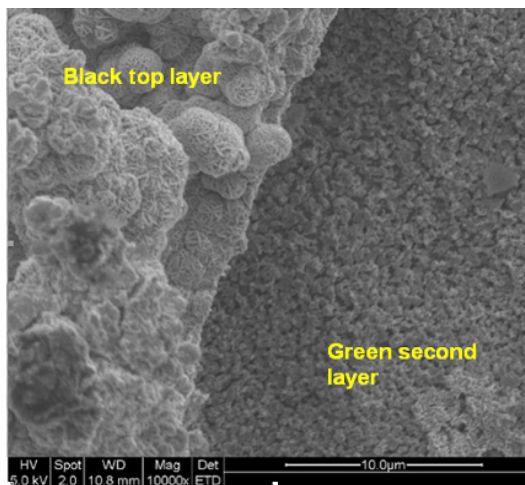


Figure 5: SEM image of CuB7B (4 weeks exposure) sample showing surface morphology.

The thickness of the reformed corrosion product was measured to be around 5 to 10 μm . Pitting corrosion of up to 20 μm deep was also observed in the cross sections. Pit area corrosion products were generally porous. EDX analysis of the corrosion products showed a mixture of copper (Cu), carbon (C), oxygen (O) with a lower level of sulphur (S) detected. The fine corrosion product layer was found to contain a higher level of sulphur.

At 13 weeks, the surface structure and composition of the corrosion product were similar to that found in the CuB7B sample. The top black layer showed a crystalline structure with a much finer morphology on the yellow second layer. The cross section showed corrosion product of a measured thickness between 10 to 50 μm . This layer appeared to be mainly cuprite (Cu_2O) which was supported by the XRD results. The corrosion product was easily flaked off and was not adherent to the metal, again showing evidence of the non-protective properties of the films.

In some areas, a layer of dark grey corrosion products formed in between the top light grey corrosion layer and the copper metal (Figure 6). This layer ranged from 50 to 100 μm in thickness and was rich in iron and contained traces of impurities such as chromium (Cr), aluminium (Al), silicon (Si), nickel (Ni) and manganese (Mn). These impurities were thought to have come from the solution having originally come from the geothermal source fluid or from the corrosion of the vessel or other test materials. The dark region appeared to be the intermediate phase in the corrosion process and was thought likely to be copper carbonate (CuCO_3), iron carbonate (FeCO_3) or iron carbide (FeC_3). However, these compounds are often amorphous and were not detected by the XRD analysis.

After 52 weeks exposure, the corrosion product was generally very voluminous and uneven, indicating a non-uniform corrosion process. The top layer of the corrosion product was porous with a denser layer underneath. It can be speculated that the bottom corrosion product contained mainly copper sulphides. However, there were areas that were yellow in colour and presence of iron oxides were possible. XRD analysis of the corrosion product collected from the surface gave a poorly crystalline spectrum but did show presence of crystalline cuprite (Cu_2O) and chalcosite (Cu_2S).

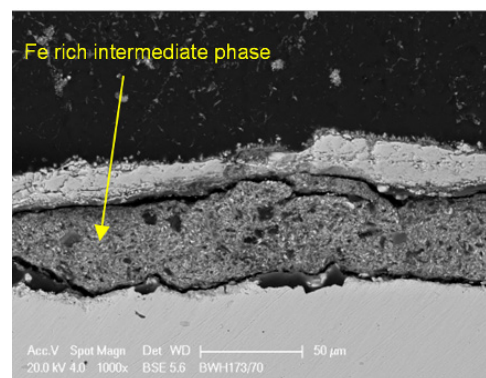


Figure 6: View of the cross section of sample CuB7D.

The CuB7H corrosion sample showed extensive flaking (Figure 7) and wasn't analysed in plan view. The cross section showed a voluminous corrosion product layer with most of the area flaked off from the metal substrate. The copper metal interface to the corrosion products was also attacked to give an open structure.

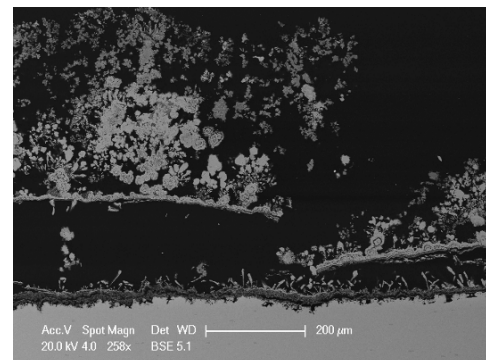


Figure 7: SEM image showing the cross section of sample CuB7H.

4.3.2 Aluminium Brass B8 Alloy Coupons

Aluminium brass coupon samples from the cold condensate environment exposed for 13 weeks (sample B8B6E) and 52 weeks (sample B8B6H) were selected for metallurgical analysis. General corrosion was observed on both samples. Sample B8B6E had a very thin and adherent corrosion product layer with the underlying copper easily visible. One side of the coupon was tarnished a grey-yellow colour, while the other side was a blue/black colour. Sample B8B6H showed a thicker dark brown corrosion product which was loosely attached.

At 13 weeks exposure the surface of corrosion product was mostly fine grained and contained mixtures of copper (Cu), zinc (Zn), sulphur (S), oxygen (O), aluminium (Al) and iron (Fe). The corrosion product structure was completely different to that seen on the pure copper sample. It formed one continuous layer of corrosion product of around 2 to 4 μm in thickness. In some areas, thicker corrosion product deposits were observed; up to 25 μm in thickness (Figure 8). The surface of the "lump" contained high levels of carbon (C), sulphur (S), copper (Cu) and iron (Fe). No zinc (Zn) or aluminium (Al) were detected. Cross section analysis of the "lump" area was conducted and showed predominance of sulphur (S), copper (Cu) and iron (Fe) which appeared to be mainly chalcopyrite. This deduction was supported by the XRD analysis.

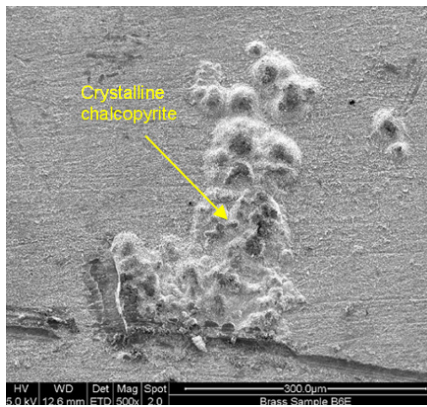


Figure 8: SEM images showing the surface and cross section of sample B8B7E.

After 52 weeks exposure, the corrosion product had changed to a fine-grained structure with many crystal growth areas (Figure 9). The fine-grained corrosion product (Figure 9) contained mixtures of copper (Cu), sulphur (S), zinc (Zn), oxygen (O), iron (Fe) and aluminium (Al), similar to those found in the 13 weeks sample. It was believed that after the longer exposure period similar chalcopyrite deposits to those observed in the sample B8B7B (13 weeks exposure) had modified into a more crystalline “spiked” structure.

The cross section analysis (Figure 9) showed a black layer in between the brass metal surface and the chalcopyrite crystals, which contained a high level of zinc.

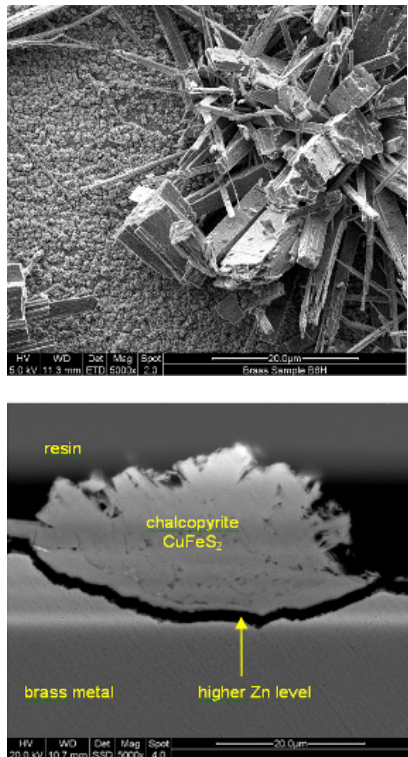


Figure 9: SEM images showing the surface and cross section of sample B8B7E.

Aluminium brass samples from exposed to aerated cold condensate environment (Vessel 7) for 4 weeks (sample B8B7B), 13 weeks (sample B8B7E) and 52 weeks (sample B8B7H) were subjected to metallurgical analysis. All of the coupons showed non-uniform corrosion with signs of air

oxidation (brown corrosion product). The corrosion product was in a layered structure. However, it was non-protective and easily flaked off. Light green coloured corrosion product was observed on some areas of sample B8B7H, indicating presence of copper carbonate or copper hydroxide (Mattsson (1980)).

At 4 weeks exposure, the inner most layer (one closest to the metal surface) was dark grey and contained a high level oxygen (O), aluminium (Al) and copper (Cu) with a lower level of sulphur (S), iron (Fe) and zinc (Zn). It is interesting to note that exceptionally high aluminium (Al) content was observed in the inner most layer (Figure 10). Aluminium (Al) was concentrated at the metal surface and formed a stable corrosion product layer. Mattsson (1980) reported that such occurrence is widely encountered for any copper alloys containing aluminium. The next layer was black coloured and contained a mixture of copper (Cu), sulphur (S) and low level of oxygen (O) and iron (Fe). This layer was less stable and had flaked off considerably. In some areas golden coloured corrosion product was observed, which contained a higher zinc (Zn) level.

The thickness of corrosion product at 4 weeks exposure was between 6 to 16 μ m and was mostly adhered to the metal surface. The cross section showed two distinct layers, a dark grey layer closest to metal surface and the top light grey (and sometime porous) corrosion product (Figure 10). The dark grey layer contained an exceptionally high level of aluminium (Al) which coincides with the surface analysis. The top light grey corrosion product contained higher levels of iron (Fe), copper (Cu) and sulphur (S). However, this layer had flaked off in some areas. The high level of iron observed in the light grey layer was thought to have been deposited from the condensate solution itself due to the corrosion of the test vessel. Again, the occurrence of iron in the solution is similar and consistent to previous analysis. EDX analysis showed a high concentration of carbon throughout the cross section, likely from the formation of copper carbonate corrosion product, however, this could not be confirmed by the XRD analysis due to the poor crystallinity of the materials.

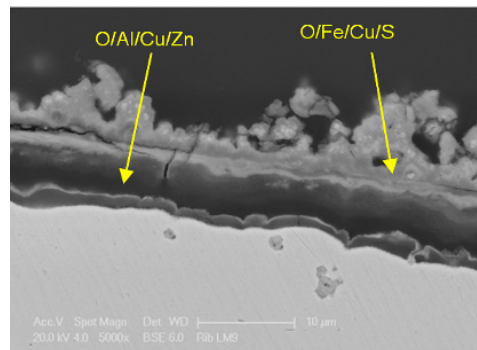


Figure 10: SEM image and elemental map of cross section of sample B8B7B.

The surface corrosion at 13 weeks exposure showed similar results to the 4 weeks sample. Corrosion was non-uniform and signs of air oxidation were apparent due to the thick brown corrosion product observed on the surface. The layer structure of the corrosion product was estimated from the surface analysis. The brown powder-like corrosion product found in the top layer contained high levels of oxygen (O) and iron (Fe) with lower levels of copper (Cu) and sulphur (S). The black second layer contained a mixture of copper (Cu), oxygen (O) and sulphur (S) with a lower level of iron

(Fe). The bottom layer contained a very high level of aluminium (Al).

The maximum thickness of the 13 weeks exposure corrosion product was around 170 μm (Figure 11). It was mainly due to the brown porous corrosion product as observed in the surface analysis (light grey in the SEM images). This layer contained a high level of iron (Fe), similar to those found in the 4 week sample. However, most of this thick layer had flaked off. The dark grey corrosion product adherent to metal surface was measured to be between 10 to 15 μm with the full layer of up to 170 μm thick. The thickness of the adherent layer did not change significantly between the 4 and 13 week exposures.

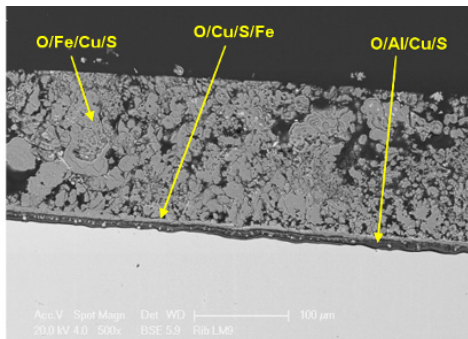


Figure 11: SEM images of the cross section of sample B8B7E.

The surface corrosion of the 52 weeks sample was again found to be similar to previous analysis of the 4 weeks and 13 weeks sample. There was a slight change in the colour of the corrosion product. The golden coloured area was no longer apparent and some areas were showing a light green coloured corrosion product. The light green colour might normally be associated with copper hydroxide or copper carbonate. However, these compounds were not detected in the XRD analysis because copper carbonate and hydroxide are often amorphous (Mattsson (1980)).

The overall corrosion product structure was non-adherent and had lost its integrity due to the prolonged exposure (Figure 12). However, two distinct layers were observed in the cross section. High aluminium (Al) content was detected in the dark grey bottom layer and it had grown to thickness between 30 to 100 μm .

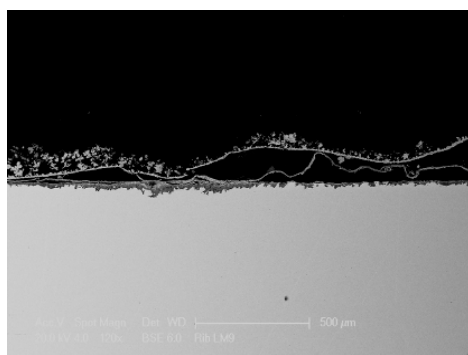


Figure 12: SEM images of cross section of sample B8B7H.

4.4 Thermodynamic Analysis

A potential-pH (Pourbaix) diagram for copper was constructed using the aid of HSC Chemistry 5 software to predict the formation of stable corrosion products. This

analysis used the conditions specific to the cold condensate environment in the Broadlands field (NZ). Only the major species found in the solution, namely copper, carbon, iron, sulphur, oxygen and hydrogen (at concentration as shown in Table 2) were inputted to the software. The free energy values used in the software's database were independently verified using available correlations. Temperature of 20°C, pressure of 300kPa and a pH range of 3.5 to 6.5 were used to simulate the condensate solution. With no oxygen leak into the system, the solution's potential would lie at the bottom limit of the $\text{H}_2\text{O}/\text{H}_2$ equilibrium line (green parallel dotted lines). The Pourbaix diagram (Figure 13) showed within the range considered, stable copper corrosion products formation would be chalcocite (Cu_2S) and bornite (Cu_3FeS_4) which is consistent with the experimental result. However, it did not predict chalcopyrite. This could be explained due to the non-uniform species' concentration inside the test vessel. Localised variability was often found, especially in crevice areas or near corroded surfaces.

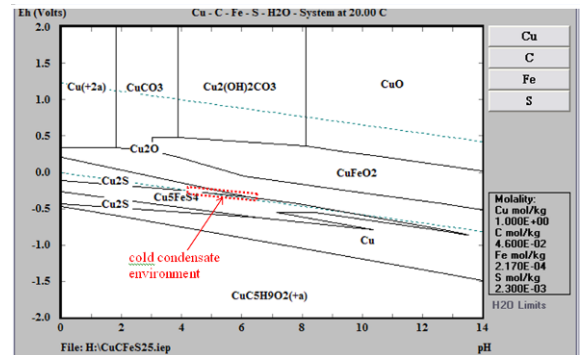


Figure 13: Pourbaix diagram of copper using the Broadlands condensate water chemistry.

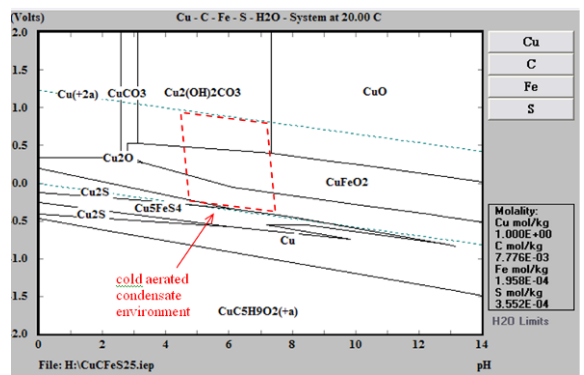


Figure 14: Pourbaix diagram for copper in the Broadlands aerated condition environment.

For the aerated conditions, a temperature of 20°C, a pressure of 135kPa and a pH range of 4.5 to 7.5 was simulated. The presence of oxygen in the system increases the potential (Eh) of the solution. It ranges from the two limits of the H_2O equilibrium line (green parallel dotted lines) as shown in Figure 14. Within the range considered, stable copper corrosion products such as chalcocite (Cu_2S), bornite (Cu_3FeS_4), cuprite (Cu_2O), malachite ($\text{Cu}_2(\text{OH})\text{CO}_3$) and cuprous ferrite (CuFeO_2) may be formed. The diagram only accurately predicts the formation of cuprite and copper sulphides. The inaccuracy is due to the local variability in the solution's concentration and the non-crystallinity of corrosion product, hence was undetected in the XRD analysis.

5 DISCUSSIONS

5.1 Corrosion of Copper in Cold Condensate

The plot of material loss due to corrosion vs. time (Figure 2) for the Broadlands well BR22 condensate environment showed linear to semi-parabolic kinetics, indicating that corrosion was controlled either by diffusion through the boundary layer or by chemical reaction rates. This suggests that long term, parabolic weight loss kinetics might be achieved. The corrosion rate of copper in Vessel 6 (Broadlands Well BR22) was relatively low compared to corrosion data that were available in literature for similar environments (Opondo (2002)). Loss of material was shown to be $0.4\mu\text{m}$ for 4 weeks exposure, while under similar environment (cold condensate at pH~5) in Okaria plant (Iceland) copper coupons showed material loss of $6.52\mu\text{m}$ after only 115.25 hours (4.8 days) exposure.

One interesting factor of this experiment was the exceptionally high soluble iron species in the condensate environments (both Vessel 6 and Vessel 7). The soluble iron species was thought to be continuously supplied to the solutions from the corrosion of the carbon steel vessel itself. The vessels were each heavily corroded under the geothermal environment and the solutions were blackened due to the iron contamination. A possible explanation for the lower corrosion rate at the Broadlands is as follows:

- Initial corrosion of copper in the condensate environment produces copper sulphide (Cu_2S) non-protective film over the metal surface.
- Soluble iron species contaminating the solution were reacting with the dissolved copper sulphide to form a variety of copper iron sulphides.
- The copper iron sulphides precipitated onto and within the copper corrosion products in the form of fine spherical agglomerates, which then transformed to a more crystalline structure over time (Figure 3 and 6). The iron rich phase on the surface of the corrosion product might act as an inhibiting boundary layer for diffusion of corrodants, which results in lower corrosion rate.
- Another explanation is that iron provided chemical reaction limiting steps in the process, with iron preferentially reacting with the copper sulphide in solution hindering the formation of new corrosion product. Iron that reacted with the corrosion product forming chalcopyrite (copper iron sulphides) over the porous copper sulphide corrosion products and protecting the film or making it more adherent. It is well known that iron acts as an inhibitor for copper corrosion in cooling waters (Nosehani (1974) and Sato (1981))).

5.2 Corrosion of Copper in Aerated Cold Condensate

The main corrosion products of copper metal predicted when exposed to aerated condensate environment were cuprite (Cu_2O) and copper sulphides. However, when oxygen was present in the aerated condition, the formed corrosion products were unstable and did not form as coherent layers. This is due to cathodic processes changing from reducing conditions where hydrogen evolution is controlling reaction rates to oxidizing conditions where hydroxide formation is the dominant cathodic reaction. Therefore, oxygen significantly increases the rate of corrosion. Inclusions of sulphur or lattice mismatch

between copper oxide and copper sulphide would also lead to structurally defective corrosion product.

This is supported by the results of the experiment. Copper exposed to the aerated condensate environment showed a higher corrosion rate compared to the non-aerated condition (Figure 2). The corrosion product layer observed was generally porous and non-protective with copper metal areas being fully exposed. Where corrosion product was adherent, cracks in the interface were commonly encountered. A high level of carbon was detected on the cross section of the sample. This occurrence could be explained due to the formation of copper carbonates or due to the diffusion of iron carbonates into the porous corrosion product. An intermediate phase of iron rich corrosion product was observed in the 13 weeks exposure period, but in this case, the presence of this phase did not reduce the corrosion rate.

5.3 Corrosion of Al Brass in Cold Condensate

The presence of Zn and other alloying elements particularly Al in the brass hindered the formation of plate-like corrosion products as seen in the pure copper sample. Alternatively, the resulting corrosion product volume was roughly equal to the metal volume, which formed a stable protective layer. This occurrence reduced the overall rate of corrosion significantly compared to the pure copper sample (see Figure 2). A thin layer of corrosion product was observed with the chalcopyrite deposits and crystalline spikes growing on the surface. The thin layer of corrosion product could not be detected in the XRD analysis due to the poor crystallinity.

The presence of iron in the solution also played a big part in the reduced of corrosion rate. It is widely known that iron species help to minimise the corrosion rate of copper and its alloys in sulphide-contaminated water. In this experiment, there is evidence of soluble iron species from the solution (due to corrosion of the vessel and other sources) reacting with the corrosion product on the surface of the brass metal to form chalcopyrite (CuFeS_2). This reaction hindered further formation of corrosion product on the metal surface and appeared to grow continuously, protecting the film layer underneath.

5.4 Corrosion of Brass in Aerated Cold Condensate

In the aerated cold condensate environment, addition of alloying elements such as zinc and aluminium to the copper did not give a significant benefit in lowering the rate of corrosion (Figure 2). The corrosion rate was high but was dominated by parabolic kinetics, which were potentially controlled by the diffusion of the corrodants though the thick corrosion product layer. This is explained by the results of the experimental analysis conducted on the samples. The corrosion products grew over time to form a thick porous layer. This layer contained high iron content, which may be acting as an inhibitor.

The role of the iron species (present as a consequence of corrosion of the test vessel) in the corrosion mechanism can be speculated to be similar to that in non-aerated solution. It provided limited protection to the corrosion layer next to the metal surface by increasing the diffusion resistance of corrodants to reach the metal surface. However, this layer was easily flaked off and did not benefit the corrosion rate in the long term. This is evidenced by the significant increase in the thickness of the dark grey corrosion layer at 52 weeks exposure. The corrosion product may have had its

integrity compromised after prolong exposure in a corrosive environment, which resulted in a non-protective layer.

6. CONCLUSIONS

The main conclusions from the evaluation of corrosion products formed on copper and brass to cold condensate and aerated cold condensate at the Broadlands Well BR22 were as follows:

COPPER – Cold Condensate

- Corrosion products formed were observed to have a plate like structure and fine spherical agglomerates, which in the long term possibly transformed to a more crystalline structure.
- Longer exposure period resulted in a thicker and more distinctive layer of corrosion product providing semi-protective properties to the copper metal substrate. In the long term, a copper sulphide layer uniformly covered the surface of the metal.
- The corrosion rate of copper was relatively low compared to literature data of similar environments due to the influence of iron. Iron species from the corrosion of the vessel reacted with the copper sulphide; forming a protective chalcopyrite (CuFeS_2) film over the porous copper sulphide corrosion product and reduce the rate of corrosion.

COPPER – Aerated Cold Condensate

- Corrosion products of copper samples exposed to the aerated condensate environment were non-uniform and were generally thicker, more fragile and readily flaked off.
- Analysis of the corrosion product showed presence of copper oxide, copper sulphide and a lower level of iron. The corrosion products were generally non-protective and readily flaked off, leaving partial or complete exposure of the metal surface.
- Intermediate phase of iron rich corrosion product was observed in the 13 weeks sample, but in this case did not reduce the rate of corrosion.

AL BRASS – Cold Condensate

- Addition of alloying elements hindered the formation of plate-like corrosion product (as observed in pure copper sample). Instead, it produced a thin and protective adherent layer of corrosion product, which reduced the corrosion rate significantly.
- The iron species acted as corrosion inhibitor (similar to the copper analysis) by reacting with copper sulphides to continuously formed copper iron sulphides. This reaction hindered further corrosion of the metal and protecting the film underneath.

AL BRASS – Aerated Cold Condensate

- The addition of oxygen into the system resulted in a thicker and more porous corrosion layer.

- Exceptionally high aluminium content was observed in the bottom layer of corrosion product. Aluminium seemed to concentrate on the metal surface and formed a stable corrosion layer to inhibit further corrosion.
- Iron species provided limited protection to the metal by forming a weak iron rich corrosion layer (increased the diffusion resistance of the corrodants to the metal surface).

Copper and its alloys have the potential to be utilised in areas where low temperature geothermal condensates are present. The addition of oxygen in the system, however, is detrimental to copper performance. Care must be taken to ensure no oxygen leakage into the system.

7. ACKNOWLEDGEMENTS

This work was undertaken under funding of New Zealand Foundation for Research Science and Technology (NZ FRST) and sponsorship from Quest Reliability Ltd and the University of Auckland. Special thanks must be addressed to Associate Professor Margaret Hyland of University of Auckland for guidance and valuable discussions throughout the project.

REFERENCES

Akol'zin, P.A., D.G. Tskhvishvili, and O.S.H. Vardigoreli, *Corrosion of Copper and its Alloys in Geothermal Waters*. Zashch Met, 1973. **9**: p. 56-58.

Braithwaite, W.R. and K.A. Lichti, *Surface Corrosion of Metals in Geothermal Fluids at Broadlands, New Zealand*. American Society for Testing and Materials, 1980. **717**: p. 81-112.

Mattsson, E., *Corrosion of Copper and Brass: Practical Experience in relation to Basic Data**. British Corrosion Journal, 1980. **15**(1): p. 6-13.

Miller, R.L., *Corrosion of Copper Base Alloys in Geothermal Brine*, in *International Symposium on Oilfield and Geothermal Chemistry 1979*, Society of Petroleum Engineers of AIME: Houston.

Nosetani, T., et al., *Comparative Corrosion Test on the Protection of Aluminimium Brass Condenser Tubes by Continuous and Intermittent Injection of Ferrous Ion*, in *Sumitomo Light Metal Techincal Reports*. 1974. p. 11-18.

Opondo, K.M., *Corrosion Test in Cooling Circuit Water at Olkaria I Plant and Scale Prediction for Olkaria and Reykjanes Fluids 2002*, The United Nations University: Reykjavík.

Rafferty, K., *Brazed plate heat exchangers for geothermal applications*. Geo-Heat Center Quarterly Bulletin, 1993. **15**(1): p. 7-12.

Rafferty, K.D., *A materials and equipment review of selected US geothermal district heating systems*. 1989, Oregon Inst. of Tech.: Klamath Falls, OR (USA). p. 383.

Sato, S., K. Nagata, and S. Yamauchi, *Evaluation of Various Preventive Measures Against Corrosion of Copper Alloy Condenser Tubes by Sea Water*. Corrosion, 1981. **81**: p. 195 (1-14).